DFT insights into the competitive adsorption of sulfur and nitrogen containing compounds and hydrocarbons on Co promoted molybdenum sulfide catalysts

Srinivas Rangarajan and Manos Mavrikakis*

Department of Chemical & Biological Engineering

University of Wisconsin-Madison, Madison WI 53706

*Corresponding author: emavrikakis@wisc.edu

ABSTRACT

Adsorption of twenty nitrogen/sulfur containing and hydrocarbon compounds on the sulfur edge of cobalt promoted molybdenum sulfide (CoMoS) catalyst was studied using density functional theory, accounting for van der Waals interactions, to elicit comparative structure-property trends across different classes of molecules relevant to hydrotreating. Unhindered organosulfur compounds preferentially adsorb on a "CUS-like" site formed by the dimerization of two neighboring sulfur atoms on the edge to create a vacancy. Nitrogen containing compounds and 4,6 dimethyldibenzothiophene, however, prefer the brim sites. Binding energy trends indicate that nitrogen containing compounds will inhibit hydrodesulfurization on the brim sites and, relatively weakly, on the CUS-like sites. Edge vacancies are, therefore, likely to be essential for hydrodesulfurization of unhindered organosulfur compounds. Further, van der Waals forces contribute significantly to the binding energy of compounds (up to 1.0 eV for large compounds such as alkyl substituted acridines) on CoMoS.

KEYWORDS: Hydrodesulfurization, CoMoS, Organonitrogen inhibition, Density functional theory, van der Waals interaction

INTRODUCTION

Hydrodesulfurization, or HDS, is a necessary industrial process to remove sulfur present as sulfides, thiols, thiophenes, and (un)substituted dibenzothiophene from gas oil feedstock[1]. Promoted molybdenum sulfides, specifically by nickel or cobalt (NiMoS/CoMoS respectively), are typical catalysts used to carry out this chemistry industrially[2]. Organonitrogen compounds such as alkyl and benzo substituted acridines and carbazoles tend to inhibit HDS under industrial conditions [3-9]. Several experimental studies have focused on assessing the impact of various organonitrogen compounds on the kinetics of HDS by cofeeding them[10] and measuring the decrease in conversion of thiophenic compounds over NiMoS and CoMoS catalysts[4, 7, 9, 11-15]. These studies also typically report adsorption/inhibition constants of these nitrogen containing compounds as they appear in simple Langmuir-Hinshelwood expressions for the overall rate of HDS reaction. Many authors have shown that such adsorption constants establish a clear trend with molecular properties such as proton affinity[4], Mulliken charge[6, 16], etc., thereby eliciting structure-property relationships. Relatively few computational chemistry studies have focused on addressing the issue of inhibition by nitrogen containing compounds. Sun et al. considered the adsorption of several organonitrogen compounds on NiMoS[17-19] and showed that the basic compounds adsorb stronger than non-basic ones on the nickel-promoted metal edges of the catalyst. Using density functional theory (DFT), Nørskov and coworkers[20] showed that Brønsted acid sites on molybdenum sulfide edges can potentially allow for protonation of basic nitrogen compounds specifically on the so-called "metal" edge; further, pyridinium adsorbs significantly more strongly than pyridine (>0.2 eV). Similar studies have not been reported for CoMoS. In a previous study[21] using DFT and accounting for van der Waals dispersive interactions, we

rigorously analyzed the adsorption of over thirty organonitrogen, organosulfur, and hydrocarbon compounds on the metal edge of NiMoS to conclude that (i) all molecules prefer to adsorb on the metal edge of NiMoS, (ii) van der Waals forces can significantly affect adsorption energies and configuration, and (iii) organonitrogen compounds block potential HDS sites and destabilize thiophene adsorption, thereby potentially inhibiting HDS.

In this work, using DFT and accounting for van der Waals dispersive interactions, we consider the adsorption of twenty organonitrogen, organosulfur, and hydrocarbon compounds on different sites of CoMoS to obtain insights into the possible modes of inhibition of HDS. Specifically, we explore: (a) the competitive adsorption potential of organonitrogen compounds and hydrocarbons vis-à-vis organosulfur compounds such as thiophene on two potential sites for HDS, (b) the destabilization of thiophene adsorption in the presence of organonitrogen compounds, and (c) the effect of van der Waals dispersion on adsorption energetics, and thereby rationalize an inhibition mechanism for HDS. We infer, thereby, the potential active site for CoMoS. We begin with a background on the state-of-the-art understanding of the catalyst structure and morphology, location and nature of active sites, and the mechanism of HDS. Subsequently, the results of our study on CoMoS and a discussion of inhibition of HDS by non-sulfur containing compounds are presented.

BACKGROUND

Bulk molybdenum sulfide (MoS_2), a transition metal dichalcogenide, is a layered material wherein each layer is composed of S-Mo-S trilayer "sandwiches". A MoS_2 catalyst particle, on

the other hand, exposes two types of edges: metal and sulfur. Spectroscopy, microscopy, and electronic structure calculations have been employed to elucidate the structure and morphology of these particles. It is established that cobalt atoms replace edge molybdenum atoms completely or partially on the sulfur edge first and then the metal edge leading to a Co-Mo-S phase[22-30]. Further, under hydrotreating conditions (specified by temperature and partial pressure of hydrogen and hydrogen sulfide gas), the edges of the catalyst particles are decorated by sulfur atoms, sulfur dimers, or sulfohydryl groups[31-40]. In addition, transmission electron microscopy (TEM) studies have shown that the number of weakly bound layers of a CoMoS catalyst particle depends on the synthesis procedure and support effects[41]. Single layered particles with minimal support interactions have been reported, especially by Topsøe and co-workers[26].

The active sites of molybdenum sulfide based catalysts are purported to be in the vicinity of the edges[41-46]. Per the traditional view, the edges are active and carbon-sulfur bond scission requires the formation of a coordinatively unsaturated site (CUS) at the edge. The incorporation of cobalt increases the formation of CUS owing to the weaker metal-sulfur bond of Co relative to Mo. Indeed, ab initio thermodynamics studies have shown that the equilibrium unpromoted sulfur edge consists of sulfur dimers bound to each Mo atom; on the other hand, the Co incorporated sulfur edge is decorated by a row of sulfur atom with a one-to-one ratio of sulfur and metal atoms. As a consequence, Co promotion potentially increases the concentration of CUS leading to higher HDS activity. Topsøe, Nørskov, Bessenbacher and coworkers have, however, shown using DFT and scanning tunneling microscopy (STM) that the "brim" of the catalyst edges possess metal-like electronic states and can activate thiophene, thereby not requiring the formation of traditional "CUS" sites[31, 44, 47, 48].

Organonitrogen compounds can adsorb on the potential active sites of CoMoS. Nørskov and coworkers showed through electronic structure calculations that specifically basic nitrogen containing compounds such as pyridine can get protonated by the hydrogen atom of the sulfohydryl groups on the unpromoted metal edges of MoS_2[20] that act as Brønsted protons, in agreement with spectroscopic evidence of pyridinium ions shown by Topsøe et al[42]. Protonation leads to relatively strong binding of the ion on the catalyst substrate in comparison to the neutral pyridine molecule. Further, STM studies have shown that pyridine adsorbs on the brim of triangular MoS_2 particles[49] only upon dosing the system with hydrogen atoms which likely creates sulfohydryl groups. A similar DFT study for CoMoS reported that sulfohydryl groups are formed under hydrotreating conditions at the sulfur edge wherein Co completely substitutes Mo atoms[50]; consequently, basic nitrogen compounds can potentially get protonated on CoMoS.

METHODS

All electronic structure calculations reported in this study were carried out on a single layer periodic stripe model consisting of four rows of six metal atoms with the top metal row being cobalt and the rest molybdenum as shown in Figure 1. The super cell includes at least 10 Å of vacuum between the adsorbate and the next periodic image in x and z directions even upon the addition of the largest molecule studied herein (diethyl acridine). To emulate the trilayer, each molybdenum row has a row of sulfur atoms on either side such that the metal atoms occupy a trigonal prismatic position with respect to the sulfur atoms with an Mo-S coordination of 6 for all atoms not located at the edges. Two catalyst models are chosen. First, the most stable

"equilibrium" edge identified by Nørskov and coworkers[49] is formed by decorating the sulfur edge at the top and metal row at the bottom by a single row of sulfur atoms, corresponding to a 50% sulfur coverage (Figure 1 left). Further, the model includes a hydrogen atom as a sulfohydryl group on the sulfur edge to represent a potential Brønsted site in view of the results reported by Nørskov and coworkers of the equilibrium edge containing one hydrogen for every four sulfur atoms on the edge (corresponding to a 25% hydrogen coverage with respect to sulfur)[50]. Our model deliberately has a lower concentration of hydrogen atoms (one in six sulfur atoms) so that the effect of a Brønsted site can be probed concurrently with a sulfur terminated site. Second, we also consider a rearranged edge (right side of Figure 1) that exposes a vacancy site where one sulfur atom has been moved to the neighboring bridge site to form a sulfur dimer. We refer to this as "*CUS-like*" owing to the non-traditional vacancy created by rearrangement as opposed to removal of sulfur atom(s) by hydrogen molecule(s). While this particular configuration is the most stable structure identified for a *CUS-like* site, the motivation for the second model arises from the preference of sulfur containing compounds to displace the edge sulfur thereby forming a sulfur dimer on the most stable edge (Figure 1 left); this is discussed in greater detail in the next section. For all molecules studied in this work, multiple adsorption configurations with respect to the stripe were considered on the brim and edges of the catalyst.

All electronic structure calculations were carried out using the plane wave density functional theory code VASP[51, 52]. In view of the large super cell size, the Brillouin zone was sampled using a Monkhorst-Pack k-point set of 1x2x1[53] and verified by convergence tests for the binding energy. The generalized gradient corrected PAW potentials[54] using the PW91 exchange correlation functional[55, 56] were used in all calculations that do not include van der Waals effects

(referred to henceforth as GGA-PW91 level of theory). A Gaussian smearing of 0.05 eV was used and all energies were extrapolated to 0 K. Plane and density wave cutoff values of 400 and 640 eV were used in all calculations with a convergence criterion for geometric relaxation being 0.02 eV/ Å. All atoms were relaxed and spin polarization and dipole corrections were included in all calculations. The lattice constant of bulk MoS_2 calculated using the PW91 functional is 3.19 Å which is comparable to the experimental value of 3.16 Å[57, 58]. The vdW-DF based optB86b-vdW functional developed by Michaelides and coworkers[59, 60] was used to estimate the effect of dispersion interactions. The lattice constant of MoS_2 calculated using this functional is 3.17 Å. The cell size for all calculations, therefore, was 27 x 19.14 (19.02) x 22.5 Å for GGA-PW91 (optB86b-vdW). In the absence of rigorous evaluation of the accuracy of this functional in the context of adsorption of large organic compounds on MoS_2 edges and terraces, we use it primarily as a means to estimate the magnitude of long range dispersion effects that are neglected using treatments at the GGA-PW91 level of theory. All gas phase calculations are carried out at the same level of theory as that of the stripe model calculations and in a rectangular box that has at least 10 Å of vacuum between images for all molecules (30 Å x 30.5 Å x 31 Å cell for molecules containing three fused rings, 20 Å x 20.5 Å x 21 Å for smaller molecules). The parameters chosen for this study were carefully checked for convergence with respect to binding energy of the largest molecule considered in this study (diethylacridine). The details of this analysis is given in the supporting information (Section 10).

The binding energy of a molecule is calculated as

$$\boldsymbol{BE = E_{molecule+stripe} - E_{molecule,\,gas} - E_{stripe}} \qquad \textbf{(1)}$$

where $\boldsymbol{E_{molecule+stripe}}$ is the total energy of the adsorbed molecule and stripe (catalyst), $\boldsymbol{E_{molecule,\,gas}}$ is the energy of gaseous molecule, and $\boldsymbol{E_{stripe}}$ is the energy of the stripe (catalyst).

RESULTS

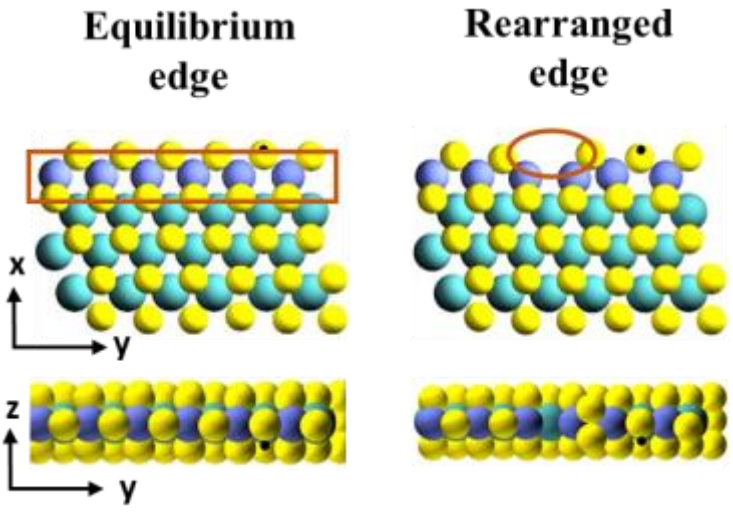

Figure 1: Catalyst models: the equilibrium edge (left) and the rearranged edge with a *CUS-like* vacant site (right). The rectangular box represents the brim region and the oval marks the *CUS-like* site. Violet (●): cobalt, cyan (●): molybdenum, yellow (●): sulfur, and black (●): hydrogen.

For all organonitrogen compounds considered in this study, the most energetically stable adsorption (at both levels of theory) was on the *brim* of the catalyst edge. Table 1, therefore, contains the binding energies of organonitrogen, organsulfur, and hydrocarbon compounds on the CoMoS brim calculated using GGA-PW91 and optB86b-vdW levels of theory. For all sulfur containing molecules, on the other hand, the most stable adsorption was on the edge with rearrangement of edge sulfur atoms to form a dimer thereby creating a *CUS-like* site. The corresponding binding energies of sulfur and nitrogen containing molecules on this edge are

given in Table 2 and the structure of the edge corresponding to this configuration is given in Figure 1(right); this restructuring of the edge decoration is endothermic from the most stable edge structure (in Figure 1(left)) by 0.96 eV at the GGA-PW91 and 0.90 eV at the optB86b-vdW level of theory. We discuss the adsorption of individual compounds below; we begin with sulfur containing compounds to lay out the benchmarks in terms of binding energy and then present other classes of compounds considered. We begin our analysis with energetics at the GGA-PW91 level of theory; unless otherwise stated explicitly, all energetics values are at the GGA-PW91 level of theory and all binding energies are reported with respect to the energy of the equilibrium edge (Figure 1 left).

Table 1: Binding energy at the GGA-PW91 and optB86b-vdW levels of theory for several compounds on the CoMoS *brim* site. The pictorial representation of the larger compounds are also given.

Compound		Binding energy BE (eV)	
		GGA-PW91	optB86b-vdW
Hydrogen[a]	H_2	-0.33	-0.25
Hydrogen sulfide	H_2S	-0.20	-0.44
Ammonia	NH_3	-0.66	-0.89
Ethane	C_2H_6	-0.07	-0.22
Ethylene	C_2H_4	-1.26	-1.50
Benzene	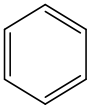	-0.13	-0.56
Toluene	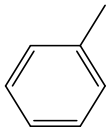	-0.16	-0.56
Aniline	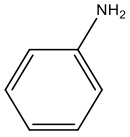	-0.40	-0.90
Pyridine	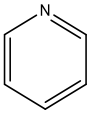	-0.76	-1.10
Pyrrole	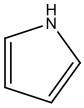	-0.21	-0.54

Lutidine	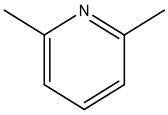	-0.87	-1.34
Quinoline	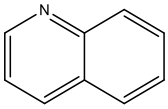	-0.86	-1.35
Indole	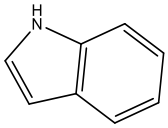	-0.18	-0.74
Acridine	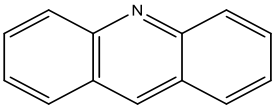	-0.90	-1.69
Carbazole	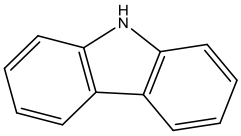	-0.19	-0.92
Dimethylacridine	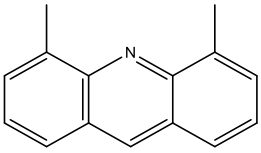	-0.87	-1.82
Dimethylcarbazole	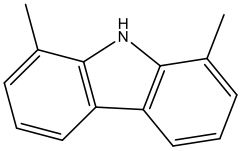	-0.22	-1.13
Diethylacridine	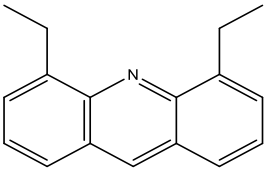	-0.95	-1.99
Thiophene		-0.14	-0.52
Dibenzothiophene	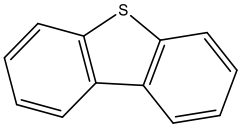	-0.19	-1.04
4,6 dimethyldibenzothiophene	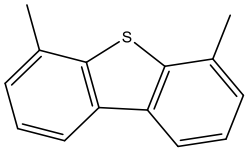	-0.20	-1.05

[a]the number given is for dissociative adsorption of hydrogen on two neighboring sulfur atoms on the sulfur edge

Table 2: Binding energy at the GGA-PW91 and optB86b-vdW levels of theory for several compounds on the CoMoS *CUS-like* edge site in configurations analogous to the most stable structure of sulfur containing compounds. The values in parenthesis are the binding energies calculated with respect to the non-equilibrium clean edge with *CUS-like* site shown in Figure 1(right).

Compound	**Binding energy BE (eV)**	
	GGA-PW91[a]	**optB86b-vdW[b]**
Hydrogen sulfide	-0.51 (-1.47)	-0.82 (-1.72)
Ammonia	-0.16 (-1.12)	-0.33 (-1.22)
Aniline	0.10 (-0.86)	-0.36 (-1.26)
Pyridine	-0.17 (-1.13)	-0.69 (-1.59)
Pyrrole	0.35 (-0.61)	-0.26 (-1.16)
Lutidine	-0.09 (-1.05)	-0.86 (-1.76)
Quinoline	-0.10 (-1.06)	-1.04 (-1.94)
Indole	0.32 (-0.64)	-0.39 (-1.29)
Acridine	0.05 (-0.91)	-0.77 (-1.67)
Carbazole	0.63 (-0.33)	-0.19 (-1.09)
Thiophene	-0.24 (-1.20)	-0.82 (-1.72)
Dibenzothiophene	-0.54 (-1.50)	-1.46 (-2.36)
4,6 dimethyldibenzothiophene	-0.31 (-1.27)	-1.28 (-2.18)

[a] the edge with *CUS-like* sites (Figure 1 right) is 0.96 eV higher in energy than the equilibrium edge using GGA-PW91 xc functional. [b]the *CUS-like* site edge is 0.90 eV higher in energy than the equilibrium edge at optB86b-vdW level of theory

Organosulfur compounds

Figure 2 shows the adsorption structure of organosulfur compounds on the *brim* of the catalyst, while Figure 3 shows the most stable adsorption structures on the catalyst edge. Alternative (side) views of these compounds are given in the supporting information (Sections 1 and 2).

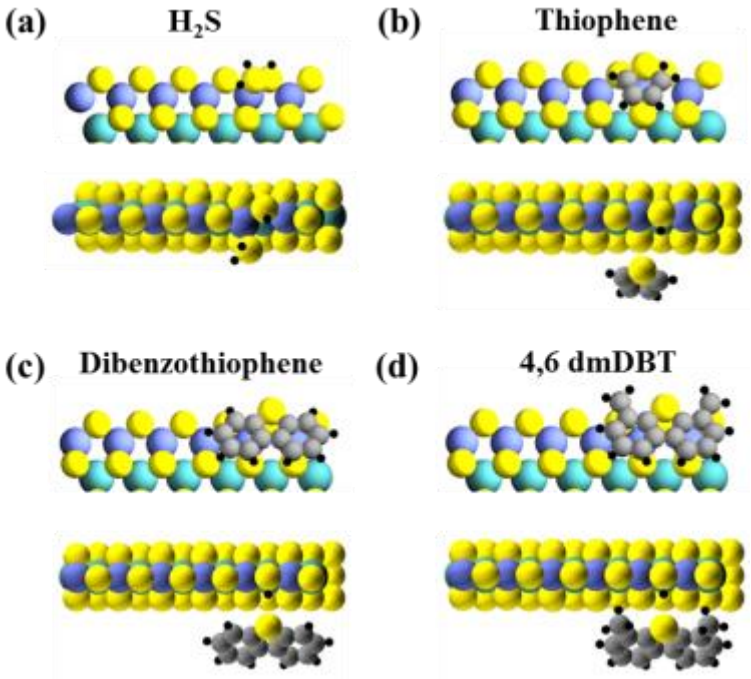

Figure 2: Most stable adsorption structures at the GGA-PW91 level of theory (front view on the top, top view on the bottom) of sulfur containing compounds on the *brim* site of the Co substituted sulfur edge of the molybdenum sulfide catalyst: (a) hydrogen sulfide, (b) thiophene, (c) dibenzothiophene, and (d) 4,6 dimethyl dibenzothiophene (4,6dmDBT). Violet (●): cobalt, cyan (●): molybdenum, yellow (●): sulfur, grey (●): carbon, and black (●): hydrogen.

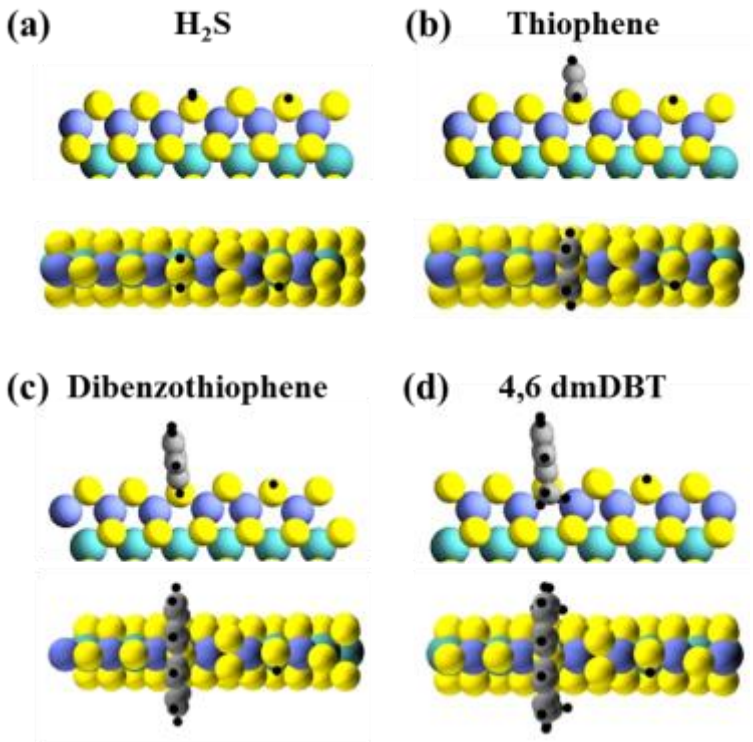

Figure 3: Most stable adsorption structures at the GGA-PW91 level of theory (front view on the top, top view on the bottom) of sulfur containing compounds on the Co substituted sulfur edge of the molybdenum sulfide catalyst: (a) hydrogen sulfide, (b) thiophene, (c) dibenzothiophene, and (d) 4,6 dimethyl dibenzothiophene. The adsorbates occupy the *CUS-like* sites formed upon restructuring the edge to form a sulfur dimer. Violet (●): cobalt, cyan (●): molybdenum, yellow (●): sulfur, grey (●): carbon, and black (●): hydrogen.

Hydrogen sulfide: Adsorption of H_2S on the *brim* site is directly on the cobalt atom next to the sulfohydryl group as shown in Figure 2(a). Other similar *brim*-site adsorption structures away from the sulfohydryl group are relatively less stable by up to 0.1 eV (at GGA-PW91), while a direct adsorption on the sulfohydryl group such that the hydrogen atom on the substrate directly points towards the sulfur atom of H_2S is essentially isoenergetic to the most stable structure in our calculations. On the other hand, the most stable adsorption structure of H_2S is on the CUS

edge as shown in Figure 3(a). This configuration is about 0.3 eV more stable than the structure in Figure 2(a) at the GGA-PW91 level of theory. This net stabilization, despite that the rearranged clean edge structure is 0.96 eV (at GGA-PW91) less stable than the most stable clean edge structure (Figure 1), reflects the high affinity of the coordinatively unsaturated site for H_2S.

Thiophene: Thiophene can adsorb on the *brim* site via the sulfohydryl group proton as shown in Figure 2(b) or on the edge site as shown in Figure 3(b). The difference between the adsorption energies at the GGA-PW91 level of theory is small, however, it is expected that the entropy loss corresponding to the latter structure is higher. The adsorption on the *brim* is such that the plane of thiophene is about 30º with respect to the plane of the CoMoS layer; the structure in Figure 3(b) is perpendicular and upright to the Cobalt-promoted sulfur edge. Nørskov and coworkers report a binding energy of -0.07 eV for thiophene adsorption[50] on the *brim* (compared to our reported value of -0.14 eV); however the specific catalyst model by the authors had a smaller supercell containing no sulfohydryl groups.

Dibenzothiophene: The adsorption structures of dibenzothiophene are similar to that of thiophene; adsorption on the *brim* is via interaction with the sulfohydryl group (Figure 2(c)) while the edge adsorption (Figure 3(c)) is perpendicular and upright with respect to the CoMoS edge and is the most stable structure for this molecule. The edge adsorption structure is stabilized more (> 0.3 eV at GGA-PW91) than the *brim* structure. The perpendicular structure on the edge may be destabilized in the presence of a support or additional CoMoS layers considering that these catalyst particles lie flat on the support and can stack up to form multilayered slabs. These

effects have not been probed in this work. However, a parallel (with respect to the edge) adsorption on the *CUS-like* site was probed; as expected the sulfur decoration on the edge hinders a Co-S bond between the cobalt atoms and dibenzothiophene (figure shown in supporting information section 4), and the binding energy (with respect to the equilibrium edge) was highly endothermic (0.86 eV). In the absence of such sulfur decorations, adsorption will potentially be stronger; in addition, corner cobalt atoms on a catalyst particle might also allow for adsorption as observed using STM[61]. These alternative sites have not been probed in this study.

4,6 dimethyldibenzothiophene: The stable adsorption structure of dimethyl substituted dibenzothiophene is similar to that of dibenzothiophene. On the *brim* site (Figure 2(d)) containing the sulfohydryl group the binding energies of both compounds are similar (-0.2 eV); on the other hand, the binding energy of adsorption on the edge site (Figure 3(d)) of 4,6 dimethyldibenzothiophene is smaller by about 0.2 eV. The relative destabilization is the effect of methyl substitution likely leading to steric hindrance. The Co-S distance between the sulfur atom of the adsorbate and the edge metal atoms increases by 0.05 Å relative to that of dibenzothiophene (2.20 Å).

Organonitrogen compounds: Basic

The adsorption structures of nitrogen containing compounds on the *brim* and *edge* site of the sulfur edge of CoMoS are given in Figures 4 and 5 respectively. The side view for *brim*

adsorption is given in the supporting information (Section 3). A detailed discussion of individual molecule adsorption modes is given below while the respective binding energies are given in Table 1 and 2.

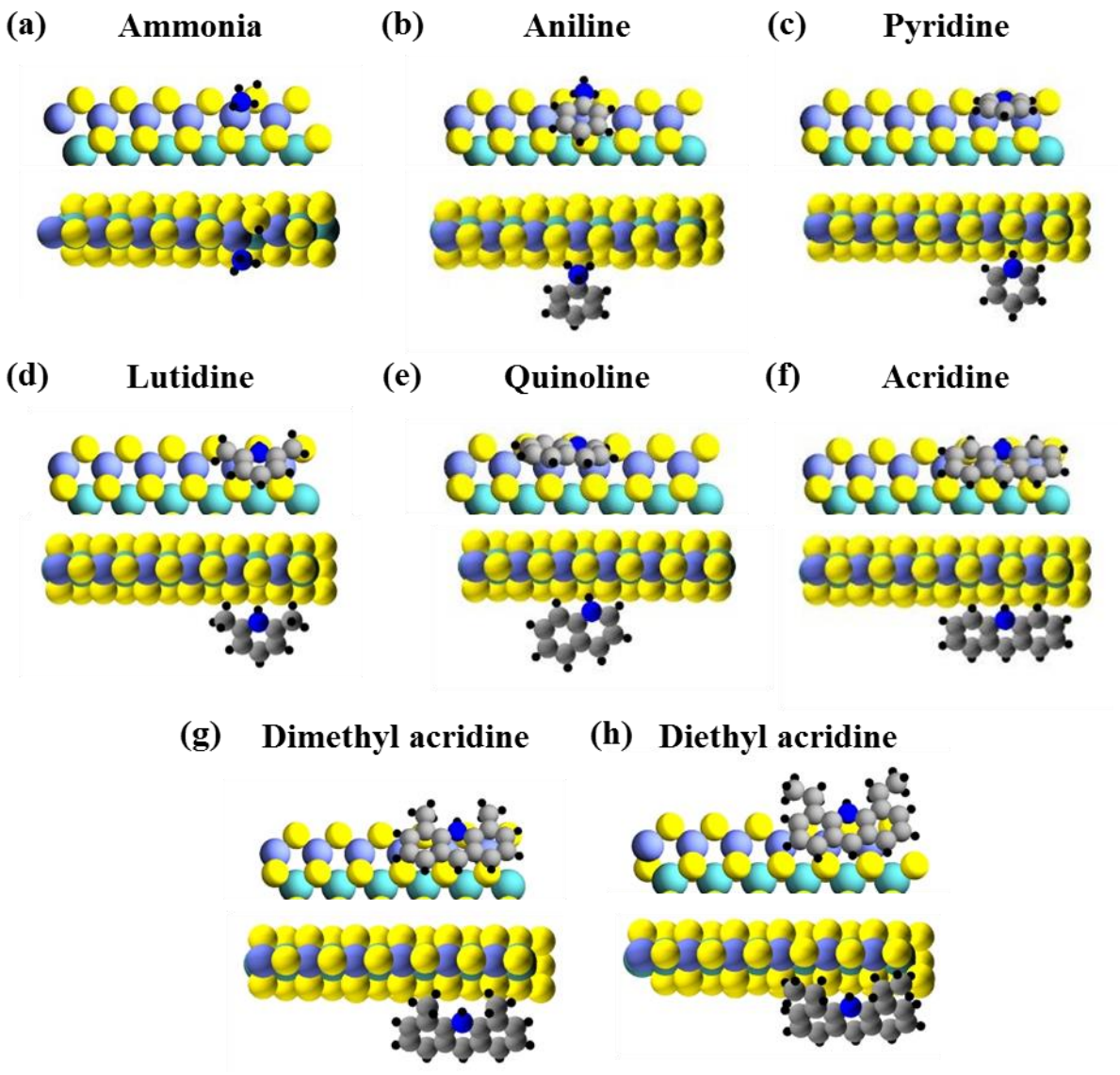

Figure 4: Most stable adsorption structures at the GGA-PW91 level of theory (front view on the top, top view on the bottom) of basic nitrogen containing compounds on the *brim* site of the Co substituted sulfur edge of the molybdenum sulfide catalyst: (a) ammonia, (b) aniline, (c) pyridine, (d) lutidine, (e) quinoline, (f) acridine, (g) dimethyl acridine, and (h) diethylacridine. Violet (●): cobalt, cyan (●): molybdenum, yellow (●): sulfur, blue (●): nitrogen, grey (●): carbon, and black (●): hydrogen.

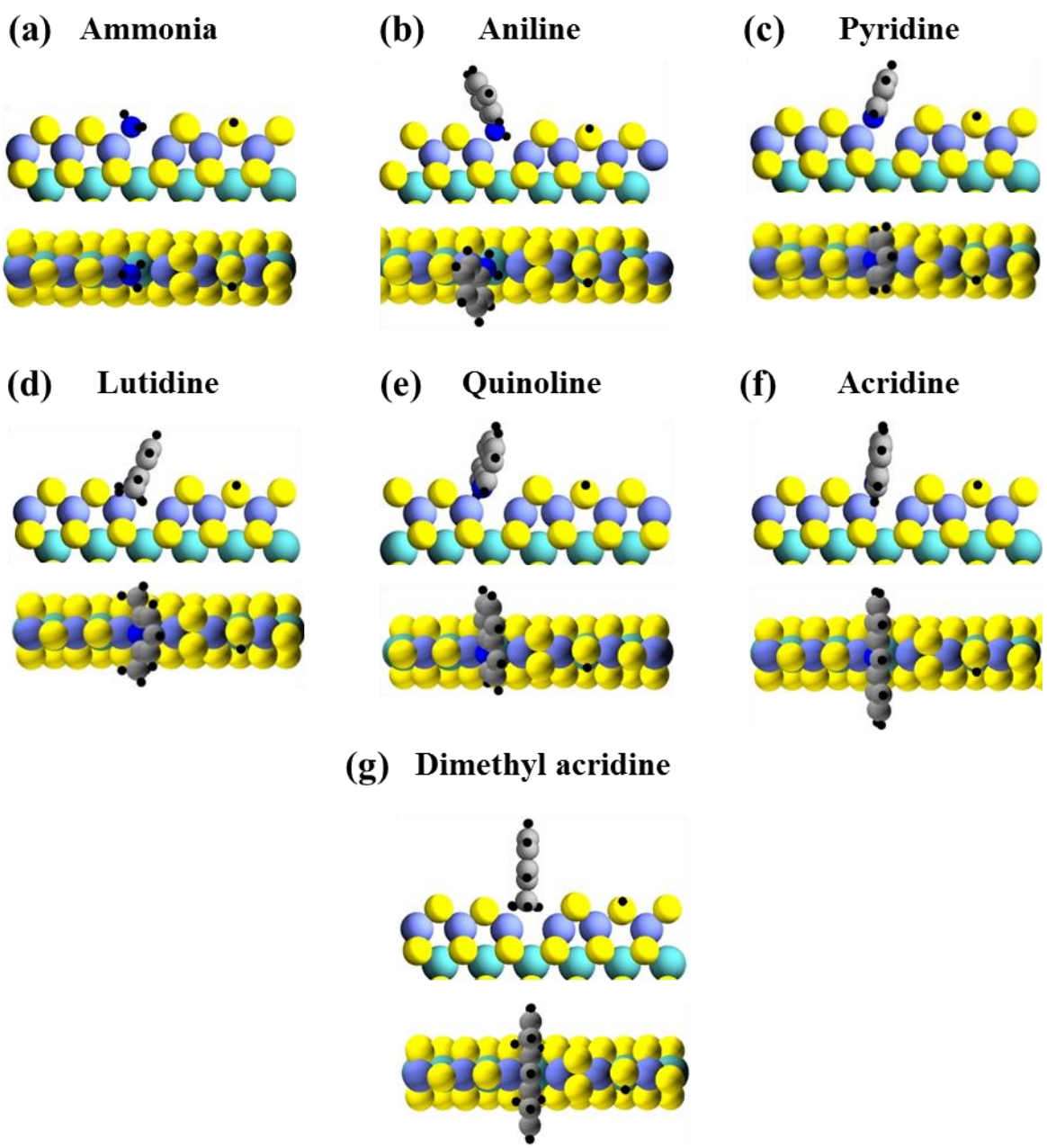

Figure 5: Most stable adsorption structures at the GGA-PW91 level of theory (front view on the top, top view on the bottom) of basic nitrogen containing compounds on the edge of the Co substituted sulfur edge of the molybdenum sulfide catalyst: (a) ammonia, (b) aniline, (c) pyridine, (d) lutidine, (e) quinoline, (f) acridine, and (g) dimethyl acridine. The adsorbates occupy the *CUS-like* sites formed upon restructuring the edge to form a sulfur dimer. Violet (●): cobalt, cyan (●): molybdenum, yellow (●): sulfur, blue (●): nitrogen, grey (●): carbon, and black (●): hydrogen.

Ammonia: In contrast to the sulfur containing compounds, the most stable adsorption structure of ammonia is on the *brim* site (Figure 4(a)), in contrast to the sulfur containing compounds, with a direct Co-N bond formation on the cobalt atom sharing the sulfohydryl group (BE of -0.66 eV at the GGA-PW91 level of theory); binding on the Co atom further away from the sulfohydryl group leads to relatively less stable adsorption by 0.1 eV. A protonated tetrahedral ammonium species adsorbing on the *brim* is relatively less stable by 0.1 eV (BE of -0.54 eV at GGA-PW91); ammonium adsorption directly on the sulfur decorated edge leads to an isoenergetic structure with respect to the *brim* with a binding energy of -0.58 eV (structures shown in the supporting information Section 4). In both cases, the ammonium species is in a bridge position between two consecutive sulfur atoms with two hydrogen atoms pointing towards them. This protonation leads to a positively charged ion as expected and is discussed in detail in a subsequent section. Adsorption on the *CUS-like* site, leading also to a direct Co-N binding (Figure 5(a)), leads to a significantly smaller binding energy value (BE = -0.16 eV with respect to the energy of the equilibrium edge).

Aniline: The most stable adsorption structure of aniline is a protonated anilinium species binding in a bridged position on the *brim* site as shown in Figure 4(b). The anilinium species has a tetrahedral geometry around the nitrogen atom and the plane of the aromatic ring is at about 30º with respect to the catalyst substrate. Non-protonated adsorption of aniline on the *brim* over the sulfohydryl group is about 0.1 eV less stable than the protonated form (structure shown in the supporting information Section 4). The adsorption on the *CUS-like* site (Figure 5(b)) is significantly less stable than on the *brim* (difference of 0.5 eV at the GGA-PW91 level of theory) making this mode of adsorption endothermic.

Pyridine: Adsorption of pyridine on the *brim* site in the form of a pyridinium ion is its most stable adsorption structure (Figure 4 (c)). The N-H bond points towards the sulfur atom (in a top-like position) and the angle between the plane of the aromatic ring and the catalyst substrate is more than 45º. Non-protonated pyridine adsorption on the *brim* is less stable by more than 0.2 eV while protonated pyridinium on the edge (in a perpendicular upright configuration relative to the sulfur-decorated edge and binding directly on sulfur as shown in the supporting information Section 4) is isoenergetic to the *brim* site (less than 0.05 eV difference in binding energy). The adsorption on the *CUS-like* site (Figure 5(c)), on the other hand, is 0.5 eV less stable although still exothermic at the GGA-PW91 level of theory. Nørskov and coworkers reported a GGA-PW91 binding energy value of pyridinium on the unpromoted metal edge of -0.59 eV[20]; adsorption on the sulfur edge as pyridinium, however, was reported to be endothermic (BE of 0.17 eV). While these two studies were not on CoMoS edges specifically, they show that pyridinium ions are preferred on the *brim* site and the formation of a pyridinium ion depends on the acidity of the proton and, therefore, on the deprotonation energy of the corresponding sulfohydryl group.

Lutidine: The most stable adsorption structure of lutidine is also a protonated lutidinium species binding on the *brim* site as shown in Figure 4(d) such that the aromatic ring is at an angle of 45º relative to the substrate, similar to that of pyridine. The binding energy of lutidine is about 0.1 eV higher than pyridine on the *brim* site at the GGA-PW91 level of theory likely because the methyl groups increase the electron density in the ring. The binding energy on the *CUS-like* edge site is lower than that on the *brim* site by more than 0.7 eV; with a BE of -0.09 eV, further,

lutidine binds weaker than pyridine on the *CUS-like* site. This weaker binding is likely due to steric hindrance. The Co-N bond distance of lutidine on this site is about 0.05 Å larger than that of pyridine (1.98 Å). The effect of alkyl substituents, therefore, has a destabilizing effect similar to that observed for organosulfur compounds.

Quinoline: The most stable adsorption structure of quinoline, similar to pyridine and lutidine, is as a protonated quinolinium ion on the *brim* site with a BE of -0.84 eV at GGA-PW91 level of theory (Figure 4 (e)). The adsorption on the *CUS-like* edge site (Figure 5 (e)) is about 0.7 eV less stable than the *brim* site.

Acridine: An acridinium ion adsorbing on the *brim* with a BE of -0.9 eV (GGA-PW91) is the most stable adsorption structure of acridine (Figure 4(f)). Adsorption on the *CUS-like* site is mildly endothermic with a BE of 0.05 eV.

Dialkylacridine: Addition of two methyl or ethyl groups to acridine at the position closest possible to the nitrogen atom creates a sterically hindered molecule similar to lutidine. The most stable adsorption structure for this compound is in the form of dialkylacridinium species on the *brim* site consistent with all the other basic nitrogen containing compounds (Figures 4g and 4f). The presence of these substituents mildly affects the binding energy with reference to acridine (BE of -0.87 eV for dimethyl acridine and -0.95 eV for diethyl acridine in comparison to -0.90 eV for acridine at GGA-PW91 level of theory). The adsorption of these compounds on the *CUS-*

like site will also likely be less stable than acridine owing to the steric effects of the alkyl substituents.

Organonitrogen compounds: Non-basic

Figures 6 and 7 show the adsorption structures of non-basic organonitrogen compounds on the *brim* and *CUS-like* edge of CoMoS; the alternative (side) view is given in supporting information (Section 3). A detailed discussion of individual adsorption modes is given below and the respective binding energies are provided in Tables 1 and 2.

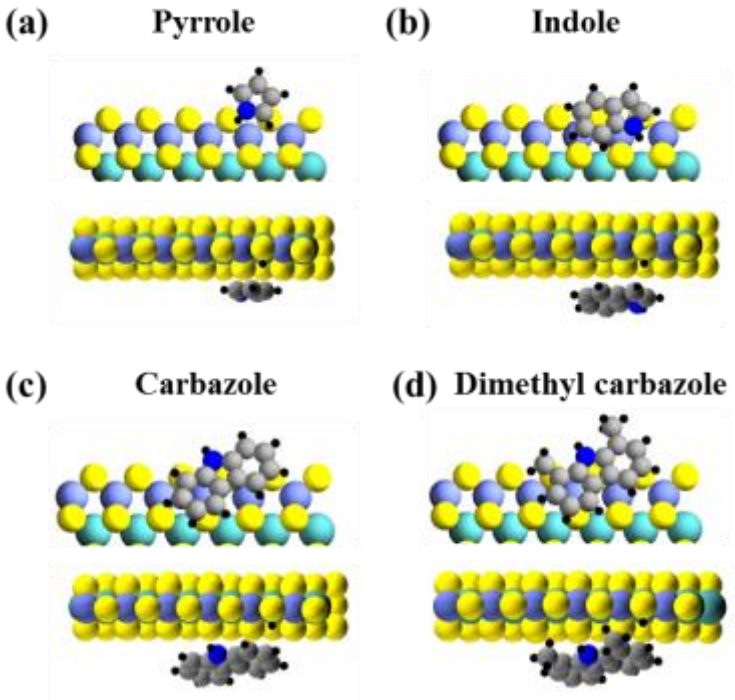

Figure 6: Most stable adsorption structures at the GGA-PW91 level of theory (front view on the top, top view on the bottom) of non-basic nitrogen containing compounds on the *brim* site of the Co substituted sulfur edge of the molybdenum sulfide catalyst: (a) pyrrole, (b) indole, (c) carbazole, and (d) dimethylcarbazole. Violet (●): cobalt, cyan (●): molybdenum, yellow (●): sulfur, blue (●): nitrogen, grey (●): carbon, and black (●): hydrogen.

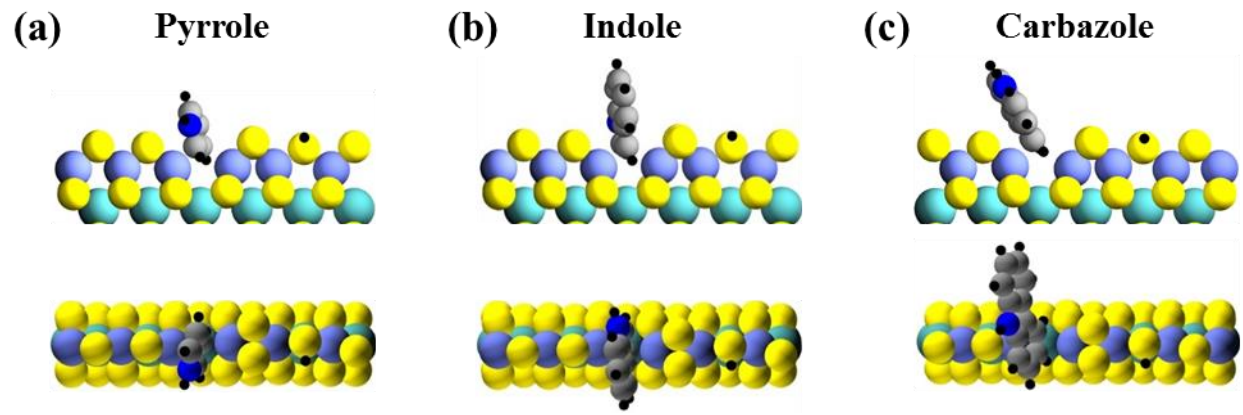

Figure 7: Most stable adsorption structures at the GGA-PW91 level of theory (front view on the top, top view on the bottom) of non-basic nitrogen containing compounds on the edge *CUS-like* site of the Co substituted sulfur edge of the molybdenum sulfide catalyst: (a) pyrrole, (b) indole, and (c) carbazole. Violet (●): cobalt, cyan (●): molybdenum, yellow (●): sulfur, blue (●): nitrogen, grey (●): carbon, and black (●): hydrogen.

Pyrrole: The most stable adsorption structure of pyrrole is on the *brim* site directly over the sulfohydryl group without being protonated (Figure 6(a)). The hydrogen of the catalyst substrate is pointing to the carbon atom adjacent to the nitrogen atoms. The binding energy of pyrrole in this configuration is -0.21 eV at the GGA-PW91 level of theory, which is significantly smaller in magnitude than pyridine. The binding angle of the plane of the aromatic ring of pyrrole with respect to the substrate, however, is much smaller than that for pyridine; pyrrole adsorbs almost parallel to the catalyst substrate. A flat adsorption structure above the sulfohydryl group on the edge of the catalyst is isoenergetic to the *brim* site. The adsorption on the *CUS-like* site (Figure 7(a)) is significantly endothermic (BE = 0.35 eV at GGA-PW91 level of theory). Pyrrole adsorbs on this site via the C-C bond interacting with Co.

Indole: The most stable adsorption structure for indole is on the *brim* site similar to that of pyrrole. The adsorption is via the carbon atom adjacent to the nitrogen atom that belongs only to the heteroaromatic ring (Figure 6(b)). The binding energy of indole is similar to that pyrrole (BE = -0.18 eV at GGA-PW91 level of theory). The adsorption on the *CUS-like* edge site (Figure 7(b)) is endothermic and is less stable than the *brim* site structure by 0.5 eV. Similar to pyrrole, indole interacts with the Co atom of the *CUS-like* site through a C-C bond of the heteroaromatic ring.

Carbazole: The adsorption of carbazole is preferred on the *brim* site via the benzene ring interacting with the sulfohydryl group (Figure 6(c)). The binding energy is -0.19 eV, which is equal to that of indole and pyrrole. The adsorption on the *CUS-like* site (Figure 7(c)) is significantly endothermic (BE = 0.63 eV at GGA-PW91 level of theory).

Dimethylcarbazole: The addition of two methyl groups in carbazole to form dimethylcarbazole does not affect the binding energy on the *brim* site (BE= -0.22 eV in comparison to BE= -0.19 eV in carbazole at GGA-PW91 level of theory). The adsorption energy and structure of dimethylcarbazole on the *CUS-like* site (not studied) is expected to be similar to that of carbazole because the methyl groups do not sterically hinder adsorption via the carbon atoms.

Hydrocarbons & hydrogen

A detailed analysis of adsorption of hydrocarbons and the hydrogen molecule are given in the supporting information (Section 11). The *brim* was the only site explored for the hydrocarbons and the binding energy values are given in Table 1. While olefins can, in principle, get protonated by the sulfohydryl group, hydrocarbons interact primarily via dispersive interactions.

Co-adsorption of Thiophene and Pyridine

Organosulfur and organonitrogen compounds compete for the CUS-like and *brim* sites although the order of preference for either sites is different for the two molecular classes. Therefore, we also studied the co-adsorption of thiophene on the *CUS-like* and *brim* sites in the presence of adsorbed pyridine, a representative organonitrogen compound, in the supercell. For this system, we calculate the co-adsorbed binding energy $BE_{coads,\,Th}$ as

$$\boldsymbol{BE_{coads,Th} = E_{thiophene+pyridine+slab} - E_{thiophene,\,gas} - E_{pyridine+slab}} \qquad \textbf{(2)}$$

where $\boldsymbol{E_{thiophene+pyridne+slab}}$ is the total energy of thiophene in the presence of adsorbed pyridine on the slab; $\boldsymbol{E_{thiophene,\,gas}}$ is the gaseous energy of the molecule, and $\boldsymbol{E_{pyridine+slab}}$ is the energy of pyridine adsorbed on the same location as in the co-adsorbed structure (which may not be the most stable adsorption structure of pyridine).

Table 3 gives the binding energy of pyridine and the corresponding $BE_{coads,\,Th}$ of thiophene values for three different co-adsorbed binding modes. It should be noted that the value of binding

energy of pyridine in each mode corresponds to the specific position and structure of its adsorption; the value in the parenthesis is the net binding energy of co-adsorbed thiophene with the most stable adsorption mode of pyridine as reference.

The three modes are: (1) adsorption of thiophene on the *brim* with pyridine on the *CUS-like* sites, (2) adsorption of thiophene on the *CUS-like* site with pyridinium on the brim, and (3) adsorption of thiophene on the *brim* with non-protonated pyridine adsorbed on the *brim*. In all three modes, the binding energy of co-adsorbed thiophene, $BE_{coads,\ Th}$, is lower than that on the clean edge, $BE_{thiophene}$. Mode 2 corresponds to the best individual adsorption structure for both thiophene and pyridine; this mode also leads to the most stable co-adsorbed mode (comparing the values given in the parenthesis). The destabilization, that is the difference between $BE_{coads,Th}$ and $BE_{thiophene}$, is 0.2 eV. Modes 1 and 3 both consider the adsorption of thiophene on the brim. For these cases, it can be noted that the individual binding energy of pyridine is significantly smaller than that of pyridinium ion on the brim and the destabilization of thiophene is negligible. The co-adsorbed binding energy of thiophene is, therefore, dependent on the position of adsorption of both adsorbates.

Table 3: The binding energy of pyridine (in the absence of thiophene) $BE_{pyridine}$, binding energy of thiophene (in the absence of pyridine) $BE_{thiophene}$, and the binding energy $BE_{coads,\ Th}$ of co-adsorbed thiophene in the presence of pyridine for three modes of co-adsorption, all calculated at the GGA-PW91 level of theory. Values in parenthesis are the net co-adsorbed binding energies with respect to the most stable adsorption mode of pyridine (as given in Table 1). All values are in eV. Violet (●): cobalt, cyan (●): molybdenum, yellow (●): sulfur, blue (●): nitrogen, grey (●): carbon, and black (●): hydrogen.

	Mode 1	Mode 2	Mode 3

	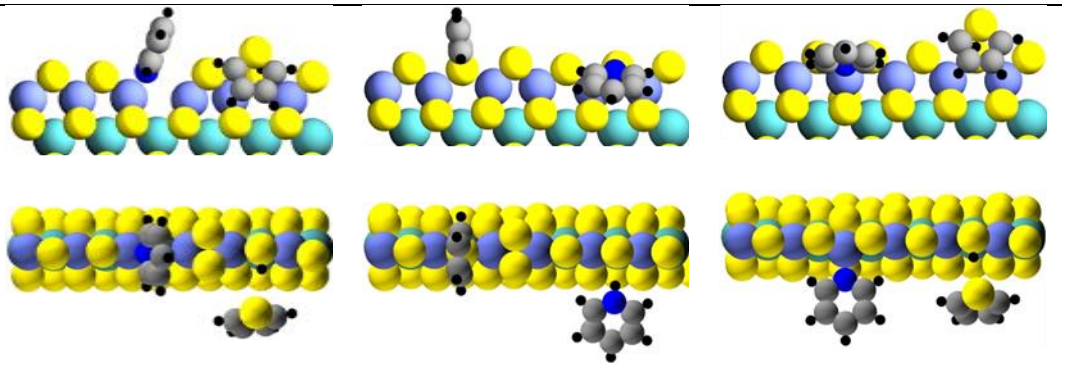		
$BE_{pyridine}$	-0.17	-0.76	-0.41
$BE_{thiophene}$	-0.14	-0.24	-0.14
$BE_{coads, Th}$	-0.13 (0.45)	-0.04 (-0.04)	-0.13 (0.21)

Effect of van der Waals stabilization

Tables 1 and 2 contain the binding energies calculated at the optB86b-vdW level of theory for *brim* and *CUS-like* site adsorption for organosulfur, organonitrogen, and hydrocarbon compounds. van der Waals stabilization progressively increases with molecular size from 0.2 eV for ammonia and hydrogen sulfide to 1 eV for acridine. Further, while the order of stability of the sites does not get altered and the adsorption structure remains very similar upon including van der Waals forces, the binding energy differences between the two sites are affected.

Sulfur-containing compounds: Inclusion of van der Waals interactions for thiophene, dibenzothiophene, and 4,6 dimethyldibenzothiophene stabilizes adsorption on both *brim* and *CUS-like* sites. Nevertheless, the binding energy on the *CUS-like* edge is larger by about 0.3, 0.4, and 0.2 eV relative to the *brim* structure.

Nitrogen containing compounds: Adsorption of ammonia is stabilized by about 0.2 eV because of van der Waals interactions; on the other hand, the stabilization is significantly larger for aniline (0.4 – 0.5 eV), pyridine (0.3 – 0.5 eV), lutidine (0.3 – 0.8 eV), quinoline (0.5 – 0.9 eV), acridine (0.8 eV), and alkyl substituted acridines (1 eV) on the *brim* and the *CUS-like edge*; this correction leads to exothermic binding energies on *CUS-like* sites in all cases in contrast to endothermic values calculated at the GGA-PW91 level of theory for many of the adsorbates.

On the *brim* site, the dispersion corrections increase the binding energy of non-basic compounds pyrrole, indole, carbazole, and dimethyl carbazole by 0.3, 0.6, 0.7, and 0.9 eV respectively. On the *CUS-like* sites, the dispersion corrections make the adsorption exothermic with the binding energy of pyrrole, indole, and carbazole being about -0.3, -0.4, and -0.2 eV respectively.

The effect of dispersion on hydrocarbons is discussed in the supporting information (Section 11). Dispersion can account for 0.2 – 0.5 eV of additional stabilization for C_2-C_6 hydrocarbons.

DISCUSSION

Formation of sulfur dimers

Sulfur containing compounds preferentially adsorb on the *CUS-like* sites of CoMoS. The formation of these sites on the clean edge involves an energy penalty of 0.96 eV; at hydrotreating conditions (673 K), the fractional concentration of such sites will, therefore, be less than 1.0×10^{-8} assuming negligible entropy change upon rearrangement (which is expected to be negative,

given the S-S bond formation). However, the relatively strong adsorption of sulfur containing compounds on these sites could still make them relevant for HDS. Our nudged elastic band (NEB) calculations for the formation of the *CUS-like* sites resulted in an energy barrier of 1.8 eV (GGA-PW91); on the other hand, NEB calculations for the formation of *CUS-like* sites and concurrent adsorption of thiophene resulted in about 0.4 eV reduction in the energy barrier (see supporting information section 7). The transition state involves the formation of a bond between the cobalt atom and the sulfur atom of thiophene. That is, the rearrangement to form the *CUS-like* sites (and the sulfur dimer) is assisted by the adsorbate, thereby leading to lower activation barriers for adsorption. In general, therefore, it is expected that the higher the interaction of the adsorbate with the cobalt atoms, the lower is the activation barrier for adsorption on *CUS-like* sites. Further, the transition state is likely to experience a greater dispersion stabilization than the initial state; the activation barrier, therefore, is expected to be even lower at the optB86b-vdW level of theory. This was inspected further by calculating single point self-consistent energy at the optB86b-vdW level of theory of the initial, final, and transition states whose structures were taken to be those obtained at the GGA-PW91 level of theory. While the intrinsic activation barrier remains unchanged because the transition state is similar to the initial state, the apparent activation barrier (with respect to gas phase thiophene and a clean slab) reduces by about 0.2 eV (details in the supporting information section 7) because of dispersive stabilization of the initial state.

Adsorption preferences of organosulfur compounds

The binding energies (in terms of the magnitude) of dibenzothiophene and 4,6 dimethyldibenzothiophene are in the order $|BE_{DBT,\ brim}| < |BE_{4,6DMDBT,\ brim}| < |BE_{4,6DMDBT,edge}| <$

|$BE_{DBT,edge}$|; both compounds prefer the *CUS-like* edge site over the *brim* site based purely on adsorption energies. On the other hand, the adsorbates retain more entropy on the brim compared to the *CUS-like* site because of higher translational entropy. Assuming that adsorbates on the *CUS-like* sites are translationally constrained while those on the *brim* retains one degree of translational entropy (along the edge) and this contributes the most to entropy differences between the two states, dibenzothiophene and its alkyl substituted derivative adsorbates on the *brim* site can have up to 40 J/mol-K higher entropy than their corresponding adsorption on *CUS-like* sites. This value is estimated to a first approximation using the one-dimensional edge translational entropy formula:

$$\boldsymbol{S_{trans,1D} = R\left(\log\left(\frac{\sqrt{2\pi mkT}}{h}\right) - \log(C_0) + 1.5\right)} \quad \textbf{(3)}$$

where C_0 is the surface concentration at saturation on the edge. For this study, we assume saturation corresponds to one-to-one ratio of adsorbate and cobalt atoms; C_0 is therefore taken to be the reciprocal of the lattice constant. This entropic difference between adsorption on these two sites leads to a free energy difference of 0.25 – 0.3 eV at hydrotreating conditions; this can compensate for the differences in binding energy for 4,6 dimethyldibenzothiophenes between *brim* and *CUS-like* sites and substituted dibenzothiophenes, in general, may preferentially adsorb on the brim sites. Dibenzothiophene, on the other hand, will adsorb preferentially via its sulfur atom on the *CUS-like* site, even upon correcting for entropy differences, thereby potentially leading to the direct activation of the C-S bond. Further, as a preliminary effort to understand the energetics of hydrodesulfurization steps of dibenzothiophene, we considered several monohydrogenated intermediates on the *brim* and *CUS-like* sites (see supporting information

section 8). The most stable monohydrogenated intermediate is the one formed in the "direct desulfurization" pathway and is located on the *CUS-like* edge. The hydrogenation step leading to this intermediate is mildly exothermic; on the other hand, all other dibenzothiophene hydrogenation steps leading to monohydrogenated intermediates either on the *brim* or the *CUS-like* sites are significantly endothermic (>0.8 eV). Further, the monohydrogenated intermediate in the hydrogenation pathway is relatively stabilized to a greater extent (0.2 eV) on the *brim* than on the *CUS-like* site. These observations indicate that the direct desulfurization pathway may be initiated on the *CUS-like* site while the hydrogenation pathway may occur on the *brim* site.

Experimental studies that show that HDS rates for alkyl substituted dibenzothiophenes are significantly lower than that of dibenzothiophene and that the latter prefers a direct desulfurization pathway on CoMoS[62, 63]. These studies have also shown that: (a) a "hydrogenation" pathway is the most likely pathway for HDS of alkyl substituted dibenzothiophenes, (b) the rate of HDS via the hydrogenation pathway is very similar in all dibenzothiophenes irrespective of alkyl substitution, and (c) H_2S inhibits the direct desulfurization pathway significantly more than the hydrogenation pathway. Further, STM studies have shown that dibenzothiophene adsorbs on the coordinatively unsaturated sites on the corners of the catalyst while 4,6 dimethyldibenzothiophene adsorbs on the *brim*. [61]

These experimental observations are in agreement with our DFT calculations and entropy arguments and leads to several propositions. First, the *direct desulfurization* pathway, which requires the activation of the C-S bond, is potentially initiated on the *CUS-like* sites; the

hydrogenation pathway, on the other hand, is initiated by the *brim* sites and is aided by the availability of protons. Dibenzothiophene preferentially adsorbs on the *CUS-like* sites and therefore undergoes HDS via the *direct desulfurization* pathway. Second, 4,6 dimethyldibenzothiophene preferentially adsorbs on the *brim* sites and therefore undergoes HDS via the *hydrogenation* pathway. Third, hydrogen sulfide also prefers *CUS-like* sites; its inhibition effect on the HDS of dibenzothiophene (via the *direct desulfurization* pathway) is, therefore, more prominent than on the HDS of 4,6 dimethyldibenzothiophene (via the *hydrogenation* pathway). Fourth, the energetics of dibenzothiophene adsorption on the *brim* site is similar to that of its substituted derivatives; the hydrogenation pathway of dibenzothiophene is, therefore, equivalent to that of 4,6 dimethyl dibenzothiophene in terms of reaction rate and inhibition by nitrogen containing compounds. Fifth, it is likely that the geometric and electronic properties of the *CUS-like* site is similar to that of the corner sites as identified in STM studies discussed earlier. The relative prominence of the corner site and the *CUS-like* site could then be a function of processing conditions, catalyst size and stacking, and the energetics associated with C-S scission on either sites.

Competitive adsorption of organonitrogen and hydrocarbon compounds

It can be inferred from Tables 1 and 2 that the adsorption of nitrogen-containing and hydrocarbon compounds depends on a variety of factors including basicity, electron density, substituent effect, steric hindrance, and size. Basic and unsaturated (containing C-C double bonds) compounds adsorb more strongly than non-basic and saturated compounds both on the *brim* and the *CUS-like* edge sites. On the brim, the Brønsted acidic proton can add on to the basic or unsaturated compound to form the cationic conjugate that is stabilized by the negatively

charged substrate; on the other hand, on the *CUS-like* site, the adsorption is akin to a Lewis acid-base coordination complex with the Co atom on the edge.

The presence of alkyl substituents on basic and non-basic compounds can lead to different consequences depending on the basicity of the compound and the site under consideration. On the *brim* site, a negligible to slight promotional effect is observed for both basic and non-basic organonitrogen compounds; the alkyl substituents tend to have an electron donating mesomeric effect that increases the electron density on the aromatic rings. On the *CUS-like* site, basic compounds with alkyl substitution are sterically hindered, which is also observed for alkyl substituted dibenzothiophene; non-basic compounds are likely not sterically hindered by alkyl groups close to the nitrogen atoms because the adsorption is via the carbon atoms on the heteroaromatic or benzene rings away from the nitrogen atoms. The size of the molecule could lead to mild steric hindrance by the carbon atoms of the adjacent aromatic rings; on the *CUS-like* site for instance, the adsorption order of basic compounds (in terms of magnitude) is $|BE_{pyridine}| > |BE_{quinoline}| > |BE_{acridine}|$ while the Co-N bond length order is pyridine (1.98 Å) < quinoline (2.0 Å) < acridine (2.06 Å) at the GGA-PW91 level of theory. A more prominent effect of size is the increasing contribution of van der Waals forces on binding as the number of dispersive atom-substrate interactions increase. For instance, at the GGA-PW91 level of theory, the binding energy of basic heteroaromatic organonitrogen compounds (pyridine, lutidine, quinoline, and acridine) differ within 0.2 eV; inclusion of van der Waals interactions, on the other hand, increases the binding energy of larger molecules relative to the smaller ones, thereby increasing the difference to about 0.6 eV. Analogously, non-basic compounds – pyrrole, indole, and carbazole – bind with similar binding energies on the brim but upon the inclusion of van der

Waals interactions they show a significant variation of about 0.4 eV (-0.54 eV for pyrrole to -0.92 eV for carbazole). On the *CUS-like* sites, the order of binding energy for the basic compounds is altered upon the inclusion of van der Waals interactions to $|BE_{pyridine}| < |BE_{acridne}| < |BE_{quinoline}|$; quinoline is stabilized the most.

Nitrogen containing compounds and hydrocarbons can inhibit hydrodesulfurization of organosulfur compounds by competitively adsorbing on the active sites. Figure 8 shows a bar graph of binding energies of organonitrogen compounds relative to thiophene, dibenzothiophene, and 4,6 dimethyldibenzothiophene on the brim and the *CUS-like* site respectively calculated using the optB86b-vdW functional. All basic heteroaromatic organonitrogen compounds (Figure 8) adsorb stronger than sulfur-containing compounds (by at least 0.3 eV with respect to thiophene) on the brim sites; non-basic compounds and aniline, on the other hand, adsorb more strongly than thiophene but bind less strongly than the larger organosulfur compounds.

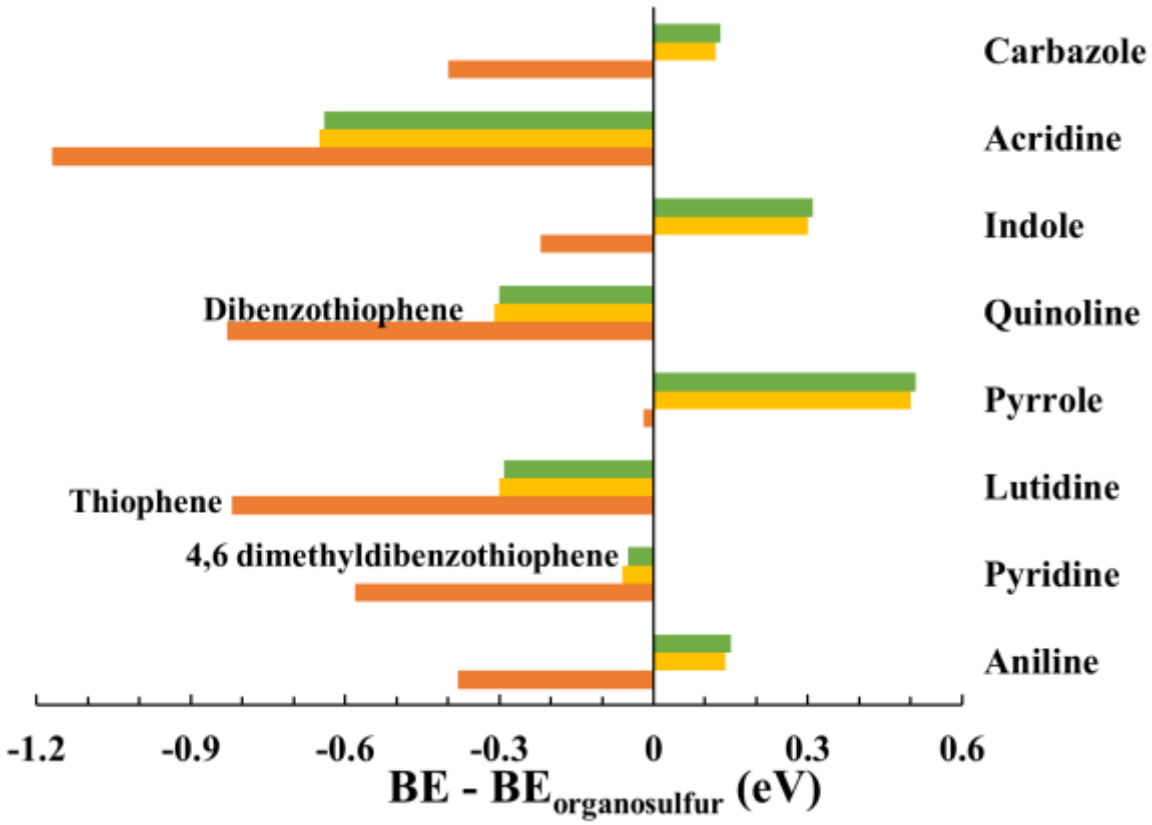

Figure 8: Relative binding energy (optB86b-vdW) bar chart for organonitrogen compounds with respect to thiophene (orange), dibenzothiophene (gold), and 4,6 dimethyldibenzothiophene (green) on the *brim* site. All values are in eV; a negative (positive) value implies the organonitrogen compound binds more (less) strongly than the organosulfur compound.

All basic compounds adsorb in the protonated form on the *brim*; these compounds, in addition, are not sterically hindered. Protonation in many cases appeared spontaneous, that is, structure relaxation calculations on many occasions led to the hydrogen atom being transferred from the substrate to the adsorbate; an NEB calculation for the protonation step also showed a spontaneous pathway from physisorbed pyridine to pyridinium ion. Further, as given in the supporting information (Section 5), the overall molecular charge from Bader charge analysis suggests that all these adsorbates, in their protonated form on the brim, are positively charged at +(0.75-0.85e). The ionic character of these adsorbates, in turn, implies that their binding energy

is related to the proton affinity of that parent compound. Figure 9 shows the binding energy at the GGA-PW91 level of theory of nitrogen containing compounds on the brim site as a function of gas phase proton affinity (obtained from NIST database[64]); this level of theory is considered to neglect the size-dependent effects of dispersion in the analysis. All heteroaromatic organonitrogen compounds follow a linear trend, as seen from the best fit line (dashed line in Figure 9) for these points. This trend line also captures the binding energy of ammonium on the brim site (which is not the most stable adsorption mode) while significantly overestimating the adsorption of aniline as anilinium ion. This discrepancy in estimating the binding energy of aniline could be due to the well-documented inaccuracies of DFT in calculating the relative gas phase reaction energies for ring and nitrogen protonation of this molecule [65-68].

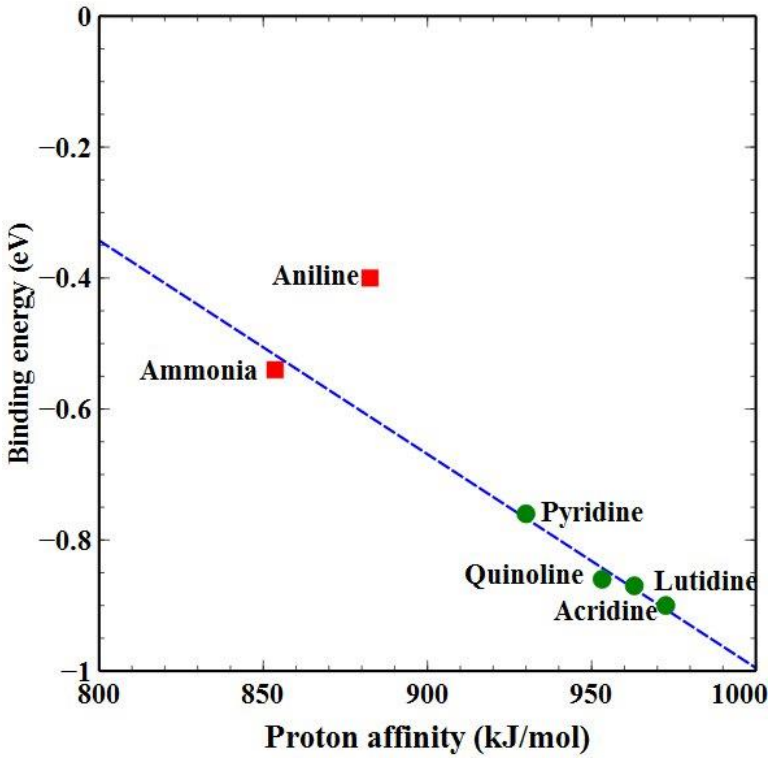

Figure 9: The binding energy-proton affinity plot for basic organonitrogen compounds adsorbed in their protonated form on the *brim* of CoMoS sulfur edge. The dashed line is a trend line based on heteroaromatic organonitrogen compounds – pyridine, quinoline, lutidine, and acridine – shown in green circles.

On the *CUS-like* site (Figure 10), organonitrogen compounds predominantly bind less strongly than organosulfur compounds barring a few exceptions such as lutidine, quinoline, and acridine vis-à-vis thiophene. While the adsorption of organonitrogen compounds on the *CUS-like* or sulfohydryl groups of the brim site inhibits direct adsorption of sulfur containing compounds on those specific sites, the presence of organonitrogen compounds on different (adjacent) sites can also indirectly influence organosulfur adsorption as evinced by the data in Table 3. The adsorption of organonitrogen compounds on the *CUS-like* site is similar to a lewis acid – base interaction. This is borne out by the linear trends (Supporting information section 9) observed between the binding energy of basic and non-basic nitrogen containing compounds on the *CUS-like* edge with their gas phase complexation energy with a Lewis acid such as aluminum chloride. Our results, therefore, suggest that the *CUS-like* site, or a geometrically and electronically equivalent site (such as corner sites with vacancy), is essential for sulfur removal from non-sterically hindered organosulfur compounds and suffers from mild inhibition by organonitrogen compounds. Further, for compounds such as dialkyl dibenzothiophene, the HDS pathway(s) can still involve the *CUS-like* site for desulfurization, subsequent to hydrogenation of an aromatic ring (likely on the brim site) that removes the steric hindrance; however, the hydrogenation step is significantly inhibited by organonitrogen compounds.

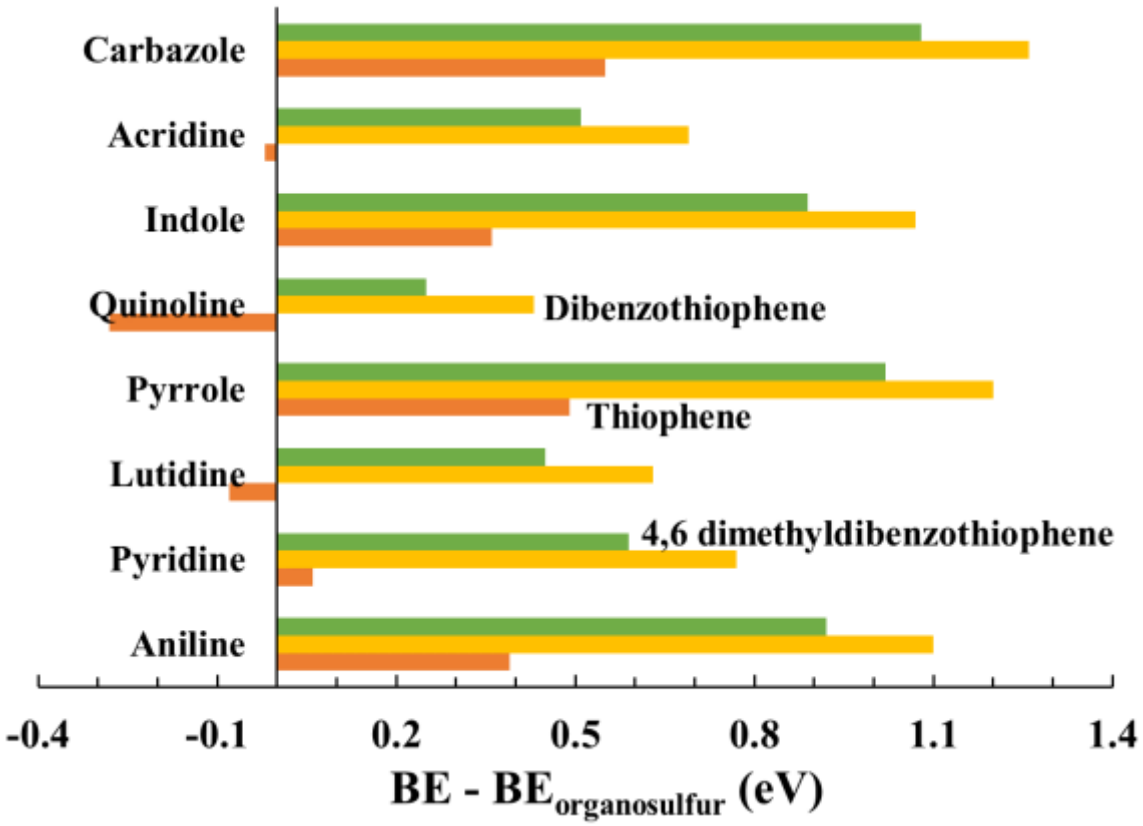

Figure 10: Relative binding energy bar chart (optB86b-vdW) for organonitrogen compounds with respect to thiophene (orange), dibenzothiophene (gold), and 4,6 dimethyldibenzothiophene (green) on the *CUS-like* site of the sulfur edge of CoMoS. All values are in eV; a negative (positive) value implies the organonitrogen compound binds more (less) strongly than the organosulfur compound.

Comparison with experiments

Experimental inhibition studies of HDS of dibenzothiophene and 4,6 dimethyldibenzothiophene on $CoMoS/Al_2O_3$ by Prins and coworkers[69] showed that methyl pyridine and methyl piperidine inhibited the hydrogenation pathway strongly while the direct desulfurization pathway was inhibited to significant but lesser extent. This is consistent with our findings. First, the basic nitrogen containing compounds adsorb on the *brim* sites more strongly than organosulfur compounds and thereby inhibit the hydrogenation pathways. Second, nitrogen containing compounds adsorb less strongly than sulfur containing compounds on the *CUS-like* sites where

direct desulfurization steps can occur; therefore their inhibitory effect on this site is significantly reduced. Further, adsorption of pyridine compounds on the brim can affect the adsorption of organosulfur compounds on the *CUS-like* sites. In a different study, Laredo et al.[14, 15] showed that inhibition of dibenzothiophene by organonitrogen compounds on $CoMoS/Al_2O_3$ followed the order indole > quinoline > carbazole. Our calculations would lead to a different order per se; specifically, quinoline would have the highest binding energy based on Table 2. The discrepancy could be due to conversion of nitrogen containing compounds to intermediates; for instance, alkyl anilines are intermediates in the hydrodenitrogenation reactions of these three compounds and their binding on the catalyst edge should follow the experimentally reported trend owing directly to steric arguments. Hydrocarbons, which are formed as intermediates in hydrodesulfurization and hydrodenitrogenation or present in the feed, can also potentially adsorb on the *brim* sites. Specifically, the strength of adsorption is in the order olefins > aromatics > alkanes on the brim; olefins can get protonated while aromatics and alkanes are predominantly stabilized by van der Waals interaction. Inhibition by hydrocarbons has been experimentally verified on CoMoS for HDS of thiophenic compounds[70, 71]. A full-fledged microkinetic model formulated on the basis of detailed mechanisms for hydrodesulfurization, hydrodenitrogenation, and hydrogenation with inputs from DFT and experiments will ultimately resolve the nature and mode of inhibition.

Infrared (IR) spectroscopy of pyridine adsorption on promoted and unpromoted MoS_2 has shown the presence of a peak at around 1545 cm^{-1} corresponding to pyridinium ion[72] and is evidence for Brønsted sites. In addition, three other peaks were found (~ 1450, 1490, and 1620 cm^{-1}) that were proposed as Lewis acid sites present on the catalyst as well as the support (as evidenced by the

presence of these peaks on sulfide alumina support). Vibrational frequencies of pyridinium adsorbed on the *brim* sites resulted in three frequencies between 1400 cm^{-1} and 1650 cm^{-1}: 1477, 1536, and 1620 cm^{-1}. The adsorbed pyridine on the *CUS-like* site also has three frequencies in this region: 1438, 1467, and 1589 cm^{-1}. Similar to the arguments made by Temel et al.[49], we propose that our value of 1536 cm^{-1} matches with the experimentally reported peak of 1545 cm^{-1} for the Brønsted site. The calculated frequency of 1438 cm^{-1} of pyridine on the *CUS-like* site is close to the experimental peak of 1450 cm^{-1} while the experimental peak at 1490 cm^{-1} is likely composed, among others, of the 1477 cm^{-1} frequency of the pyridinium ion on the brim and 1467 cm^{-1} frequency of pyridine on the *CUS-like* site. Finally, the experimental peak at 1620 cm^{-1} is composed, among others, the 1589 cm^{-1} and 1620 cm^{-1} frequencies of pyridine on the *CUS-like* site and pyridinium on the *brim* site respectively.

Effect of the liquid phase

Industrial hydrotreaters are trickle bed reactors and have a liquid phase. It is, therefore, pertinent to consider the effect of the presence of a liquid phase on the adsorption of organosulfur and organonitrogen compounds in gas oil feeds onto CoMoS sites. The liquid phase, comprising primarily of hydrocarbons – alkanes, olefins, naphthenics, and aromatics – can influence adsorption and reactions on CoMoS active sites in multiple ways. First, organosulfur and organonitrogen compounds can be solvated in the liquid. Indeed, the experimental solvation enthalpy of thiophene and pyridine in hexadecane (and other hydrocarbon solvents) is about 30 kJ/mol; the solvation enthalpy further increases with the size of the solute. Second, hydrocarbon compounds in the liquid phase can compete with organosulfur and organonitrogen compounds for active sites on CoMoS and thereby inhibit their adsorption and subsequent reaction. This

inhibition, however, is less pronounced when organosulfur and organonitrogen compounds bind through covalent bonds and are not just physisorbed because hydrocarbons interact with the surface primarily via van der Waals interaction (supporting information section 11). The liquid phase, in principle, can also solvate the adsorbed intermediates. Such effects can be explored through implicit solvation models or through explicitly including multiple molecules of representative hydrocarbon compounds into the model system. Such analyses is beyond the scope of this work. While all these factors can affect the adsorption energetics on CoMoS, the effect is likely minimal because the liquid phase is largely composed of aprotic nonpolar hydrocarbon compounds and the nature of their interaction with solutes is primarily dispersive.

Conclusions

The adsorption of nitrogen containing and hydrocarbon compounds were studied in comparison to that of sulfur containing compounds on cobalt promoted molybdenum sulfide catalyst using periodic DFT with the GGA-PW91 level of theory and DFT with van der Waals interactions at the optB86b-vdW level of theory. We find that: (a) unhindered sulfur containing compounds including H_2S, thiophene, and dibenzothiophene adsorb stronger on a CUS-like site formed by rearrangement of sulfur atoms decorating the Co-promoted sulfur edge of the catalyst, (b) organonitrogen compounds and ammonia prefer the brim site for adsorption, (c) basic nitrogen containing compounds prefer to be protonated by a sulfohydryl proton on sulfur edge forming a cation (d) van der Waals interactions significantly alter binding energetics (by up to 1.0 eV), (e) olefins also bind strongly on the brim by forming alkyl sulfides, and (f) the presence of pyridine in particular, and nitrogen containing compounds in general, destabilizes adsorption of thiophene on the CUS-like sites. We further suggest that thiophene and dibenzothiophene can undergo

hydrodesulfurization via direct desulfurization pathway on the CUS-like site while 4,6 dimethyl dibenzothiophene prefers a hydrogenation pathway on the brim sites. Nitrogen containing compounds were found to inhibit the hydrogenation pathway more than the direct desulfurization pathway, as observed experimentally, because they prefer the brim over the CUS-like sites.

Supplementary Information Available: Alternative views of organosulfur and organonitrogen compounds on edge and brim sites of CoMoS, Bader charge analysis, alternative ethylene adsorption structure, nudged elastic band calculations for CUS-like site formation and pyridine protonation, energetics of monohydrogenation of dibenzothiophene on CoMoS, complexation energy with $AlCl_3$ as a descriptor for adsorption on CUS-like sites, analysis of convergence of the binding energy of diethylacridine, and adsorption of hydrocarbons and hydrogen on CoMoS. This material is available free of charge via the Internet at http://pubs.acs.org."

Acknowledgements: The authors acknowledge partial financial support from BP Products North America Inc. and specifically thank Drs. Hong Yang, Corneliu Buda, Dong Wang, and Phil Sinclair for valuable discussions during the course of this work. The authors also thank Yunhai Bai, Sha Li, and Anthony Plauck for valuable comments on the manuscript. Financial support from Department of Energy-Basic Energy Sciences, Division of Chemical Sciences (DE-FG02-05ER15731) is also acknowledged. The computational work was performed partly using supercomputing resources at EMSL, a national scientific user facility at Pacific Northwest national lab (PNNL), the center for nanoscale materials (CNM) at Argonne national lab (ANL), and the national energy research scientific computing center (NERSC). EMSL is sponsored by

the Department of Energy's Office of Biological and Environmental Research located at PNNL. CNM and NERSC are supported by the U.S. Department of Energy, Office of Science, under contracts DE-AC02-06CH11357 and DE-AC02-05CH11231, respectively. This research was also partially performed using the compute resources and assistance of the UW-Madison Center for High Throughput Computing (CHTC) in the Department of Computer Sciences. The CHTC is supported by UW-Madison, the Advanced Computing Initiative, the Wisconsin Alumni Research Foundation, the Wisconsin Institute for Discovery, and the National Science Foundation, and is an active member of the Open Science Grid, which is supported by the National Science Foundation and the U.S. Department of Energy's Office of Science.

References

1. Ho, T. C., *Catal. Today* **2004,** 98, 3-18.
2. Stanislaus, A.; Marafi, A.; Rana, M. S., *Catal. Today* **2010,** 153, 1-68.
3. Prins, R.; Egorova, A.; Rothlisberger, A.; Zhao, Y.; Sivasankar, N.; Kukula, P., *Catal. Today* **2006,** 111, 84-93.
4. Lavopa, V.; Satterfield, C. N., *J. Catal.* **1988,** 110, 375-387.
5. Girgis, M. J.; Gates, B. C., *Ind. Eng. Chem. Res.* **1991,** 30, 2021-2058.
6. Beltramone, A. R.; Crossley, S.; Resasco, D. E.; Alvarez, W. E.; Choudhary, T. V., *Catal. Lett.* **2008,** 123, 181-185.
7. Yang, H.; Chen, J. W.; Fairbridge, C.; Briker, Y.; Zhu, Y. J.; Ring, Z., *Fuel Process. Technol.* **2004,** 85, 1415-1429.
8. Kwak, C.; Lee, J. J.; Bae, J. S.; Moon, S. H., *Appl. Catal., B* **2001,** 35, 59-68.
9. Nagai, M.; Sato, T.; Aiba, A., *J. Catal.* **1986,** 97, 52-58.
10. Zeuthen, P.; Knudsen, K. G.; Whitehurst, D. D., *Catal. Today* **2001,** 65, 307-314.
11. Egorova, M.; Prins, R., *J. Catal.* **2004,** 224, 278-287.
12. Egorova, M.; Prins, R., *J. Catal.* **2004,** 221, 11-19.
13. Laredo, G. C.; Montesinos, A.; De los Reyes, J. A., *Appl. Catal., A* **2004,** 265, 171-183.
14. Laredo, G. C.; Altamirano, E.; De los Reyes, J. A., *Appl. Catal., A* **2003,** 243, 207-214.
15. Laredo, G. C.; De los Reyes, J. A.; Cano, J. L.; Castillo, J. J., *Appl. Catal., A* **2001,** 207, 103-112.
16. Sun, M.; Nelson, A. E.; Adjaye, J., *J. Mol. Catal. A: Chem.* **2004,** 222, 243-251.
17. Sun, M. Y.; Nelson, A. E.; Adjaye, J., *Catal. Lett.* **2006,** 109, 133-138.
18. Sun, M. Y.; Nelson, A. E.; Adjaye, J., *J. Catal.* **2005,** 231, 223-231.
19. Sun, M. Y.; Nelson, A. E.; Adjaye, J., *Catal. Today* **2005,** 109, 49-53.

20. Logadottir, A.; Moses, P. G.; Hinnemann, B.; Topsoe, N. Y.; Knudsen, K. G.; Topsoe, H.; Nørskov, J. K., *Catal. Today* **2006,** 111, 44-51.
21. Rangarajan, S.; Mavrikakis, M., *AIChE J.* **2015**, 61, 4036-4050.
22. Byskov, L. S.; Nørskov, J. K.; Clausen, B. S.; Topsoe, H., *J. Catal.* **1999,** 187, 109-122.
23. Schweiger, H.; Raybaud, P.; Toulhoat, H., *J. Catal.* **2002,** 212, 33-38.
24. Krebs, E.; Silvi, B.; Raybaud, P., *Catal. Today* **2008,** 130, 160-169.
25. Lauritsen, J. V.; Kibsgaard, J.; Olesen, G. H.; Moses, P. G.; Hinnemann, B.; Helveg, S.; Nørskov, J. K.; Clausen, B. S.; Topsoe, H.; Laegsgaard, E.; Besenbacher, F., *J. Catal.* **2007,** 249, 220-233.
26. Topsoe, H., *Appl. Catal., A* **2007,** 322, 3-8.
27. Kibsgaard, J.; Tuxen, A.; Knudsen, K. G.; Brorson, M.; Topsøe, H.; Laegsgaard, E.; Lauritsen, J. V.; Besenbacher, F., *J. Catal.* **2010,** 272, 195-203.
28. Nelson, A. E.; Sun, M.; Junaid, A. S. M., *J. Catal.* **2006,** 241, 180-188.
29. Topsøe, N. Y.; Topsøe, H., *J. Catal.* **1983,** 84, 386-401.
30. Gandubert, A. D.; Krebs, E.; Legens, C.; Costa, D.; Guillaume, D.; Raybaud, P., *Catal. Today* **2008,** 130, 149-159.
31. Bollinger, M. V.; Jacobsen, K. W.; Nørskov, J. K., *Phys. Rev. B* **2003,** 67, 085410.
32. Hinnemann, B.; Nørskov, J. K.; Topsøe, H., *J. Phys.Chem. B* **2005,** 109, 2245-2253.
33. Prodhomme, P.-Y.; Raybaud, P.; Toulhoat, H., *J. Catal.* **2011,** 280, 178-195.
34. Schweiger, H.; Raybaud, P.; Kresse, G.; Toulhoat, H., *J. Catal.* **2002,** 207, 76-87.
35. Raybaud, P.; Hafner, J.; Kresse, G.; Kasztelan, S.; Toulhoat, H., *J. Catal.* **2000,** 190, 128-143.
36. Raybaud, P.; Hafner, J.; Kresse, G.; Toulhoat, H., *Stud. Surf. Sci. Catal.* **1999,** 127, 309-317.
37. Paul, J. F.; Payen, E., V., *J. Phys.Chem. B* **2003,** 107, 4057-4064.
38. Cristol, S.; Paul, J. F.; Payen, E.; Bougeard, D.; Clemendot, S.; Hutschka, F., *J. Phys.Chem. B* **2002,** 106, 5659-5667.
39. Travert, A.; Nakamura, H.; van Santen, R. A.; Cristol, S.; Paul, J. F.; Payen, E., *J. Am. Chem. Soc.* **2002,** 124, 7084-7095.
40. Cristol, S.; Paul, J. F.; Payen, E.; Bougeard, D.; Clemendot, S.; Hutschka, F., *J. Phys.Chem. B* **2000,** 104, 11220-11229.
41. Berhault, G.; De la Rosa, M. P.; Mehta, A.; Yacaman, M. J.; Chianelli, R. R., *Appl. Catal., A* **2008,** 345, 80-88.
42. Topsøe, H.; Clausen, B. S., *Appl. Catal.* **1986,** 25, 273-293.
43. Lauritsen, J. V.; Bollinger, M. V.; Laegsgaard, E.; Jacobsen, K. W.; Nørskov, J. K.; Clausen, B. S.; Topsøe, H.; Besenbacher, F., *J. Catal.* **2004,** 221, 510-522.
44. Besenbacher, F.; Brorson, M.; Clausen, B. S.; Helveg, S.; Hinnemann, B.; Kibsgaard, J.; Lauritsen, J. V.; Moses, P. G.; Nørskov, J. K.; Topsøe, H., *Catal. Today* **2008,** 130, 86-96.
45. Kasztelan, S.; Toulhoat, H.; Grimblot, J.; Bonnelle, J. P., *Appl. Catal.* **1984,** 13, 127-159.
46. Daage, M.; Chianelli, R. R., *J. Catal.* **1994,** 149, 414-427.
47. Hinnemann, B.; Moses, P. G.; Nørskov, J. K., *J. Phys. Condens. Matter* **2008,** 20, 062436.
48. Moses, P. G.; Hinnemann, B.; Topsøe, H.; Nørskov, J. K., *J. Catal.* **2008,** 260, 202-203.
49. Temel, B.; Tuxen, A. K.; Kibsgaard, J.; Topsøe, N.-Y.; Hinnemann, B.; Knudsen, K. G.; Topsøe, H.; Lauritsen, J. V.; Besenbacher, F., *J. Catal.* **2010,** 271, 280-289.
50. Moses, P. G.; Hinnemann, B.; Topsøe, H.; Nørskov, J. K., *J. Catal.* **2009,** 268, 201-208.
51. Kresse, G.; Furthmuller, J., *Comput. Mater. Sci.* **1996,** 6, 15-50.
52. Kresse, G.; Furthmuller, J., *Phys. Rev. B* **1996,** 54, 11169-11186.
53. Monkhorst, H. J.; Pack, J. D., *Phys. Rev. B* **1976,** 13, 5188-5192.
54. Kresse, G.; Joubert, D., *Phys. Rev. B* **1999,** 59, 1758-1775.
55. Perdew, J. P.; Chevary, J. A.; Vosko, S. H.; Jackson, K. A.; Pederson, M. R.; Singh, D. J.; Fiolhais, C., *Phys. Rev. B* **1993,** 48, 4978-4978.

56. Perdew, J. P.; Chevary, J. A.; Vosko, S. H.; Jackson, K. A.; Pederson, M. R.; Singh, D. J.; Fiolhais, C., *Phys. Rev. B* **1992,** 46, 6671-6687.
57. Raybaud, P.; Kresse, G.; Hafner, J.; Toulhoat, H., *J. Phys. Conden. Matter* **1997,** 9, 11085-11106.
58. Raybaud, P.; Hafner, J.; Kresse, G.; Toulhoat, H., *J. Phys. Conden. Matter* **1997,** 9, (50), 11107-11140.
59. Klimes, J.; Bowler, D. R.; Michaelides, A., *Phys. Rev. B* **2011,** 83, 195131.
60. Klimes, J.; Bowler, D. R.; Michaelides, A., *J. Phys. Conden. Matter* **2010,** 22, 022201.
61. Tuxen, A. K.; Fuchtbauer, H. G.; Temel, B.; Hinnemann, B.; Topsøe, H.; Knudsen, K. G.; Besenbacher, F.; Lauritsen, J. V., *J. Catal.* **2012,** 295, 146-154.
62. Gates, B. C.; Topsøe, H., *Polyhedron* **1997,** 16, 3213-3217.
63. Egorova, M.; Prins, R., *J. Catal.* **2004,** 225, 417-427.
64. NIST NIST Webbook (http://webbook.nist.gov/chemistry/). http://webbook.nist.gov/chemistry/ (Mar 27, 2015),
65. Russo, N.; Toscano, M.; Grand, A.; Mineva, T., *J. Phys. Chem. A* **2000,** 104, 4017-4021.
66. Boese, A. D.; Martin, J. M. L.; De Proft, F.; Geerlings, P., *ACS Symposium Series* **2007,** 958, 183-192.
67. Hillebrand, C.; Klessinger, M.; EckertMaksic, M.; Maksic, Z. B., *J. Phys. Chem.* **1996,** 100, 9698-9702.
68. Maksic, Z. B.; Kovacevic, B.; Vianello, R., *Chem. Rev.* **2012,** 112, 5240-5270.
69. Egorova, M.; Prins, R., *J. Catal.* **2006,** 241, 162-172.
70. Morales-Valencia, E. M.; Baldovino-Medrano, V. G.; Giraldo, S. A., *Fuel* **2015,** 153, 294-302.
71. Hatanaka, S.; Yamada, M.; Sadakane, O., *Ind. Eng. Chem. Res.* **1997,** 36, 5110-5117.
72. Topsøe, N. Y.; Topsøe, H.; Massoth, F. E., *J. Catal.* **1989,** 119, 252-255.

TOC Figure

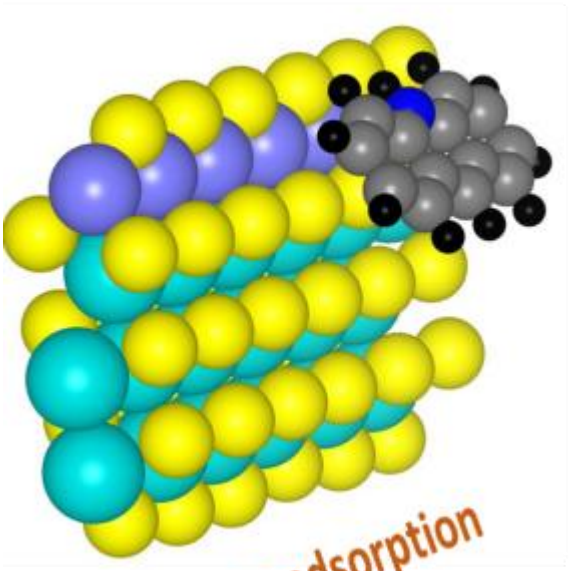

Brim adsorption

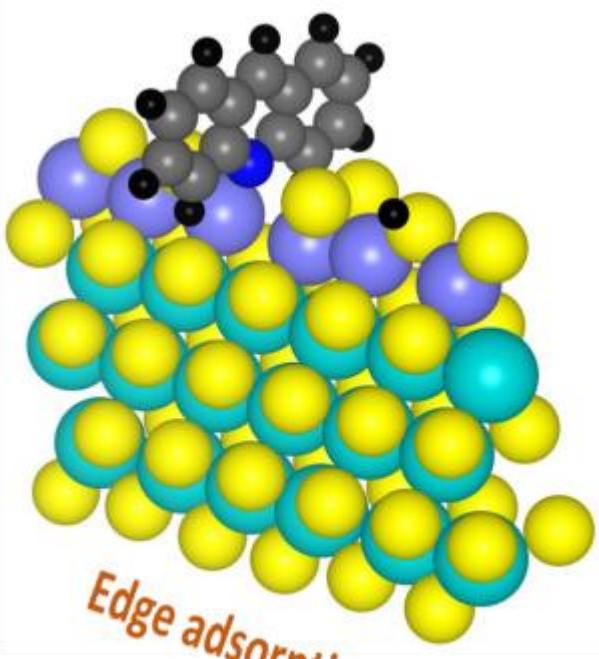

Edge adsorption